Terahertz metamolecules deposited on thin flexible polymer: design, fabrication and experimental characterization

Riad Yahiaoui, Keisuke Takano, Fumiaki Miyamaru, Masanori Hangyou, Patrick Mounaix

Terahertz metamolecules deposited on thin flexible polymer: design, fabrication and experimental characterization

2014 J. Opt. 16 094014

(http://iopscience. op.o g/2040-8986/16/9/094014)

Terahertz metamolecules deposited on thin flexible polymer: design, fabrication and experimental characterization

R Yahiaoui[1], K Takano[2], F Miyamaru[3], M Hangyo[2] and P Mounaix[4]

[1] XLIM, Univ. Limoges, CNRS, UMR 6172, 7 rue Jules Vallès, F 19100 Brive, France
[2] Institute of Laser Engineering, Osaka University, 2 6 Yamadaoka, Suita, Osaka 565 0871, Japan
[3] Department of Physics, Faculty of Science, Shinshu University, Nagano 390 8621, Japan
[4] LOMA, Univ. Bordeaux, CNRS, UMR 5798, 351 Cours de la Libération, F 33405 Talence Cedex, France

E mail: riad.yahiaoui@unilim.fr

Abstract

Metamolecules deposited on thin dielectric film using standard optical lithography have been investigated numerically and experimentally in the terahertz regime. The topology of the proposed metamolecules is able to achieve a multiple band frequency response over a broad frequency range. The analysis of the spectral response of the investigated metamaterial reveals that such a feature arises from coupling effects between its individual constituents. The successful demonstration of a THz flexible metamaterial may open up new perspectives towards achieving complex electromagnetic functions involving non-planar metamaterials with simple design and fabrication.

Keywords: metamaterials, coupling mechanisms, terahertz time domain spectroscopy

1. Introduction

Metamaterials have grown substantially within the scientific community due to their unusual properties and their ability to control electromagnetic waves in an amazing manner [1, 2]. Usually based on dielectric particles or metallodielectric composite structured on a size scale much smaller than the wavelength of external stimuli, they are increasingly used to achieve various electromagnetic functions such as absorption, radiation, filtering, coupling, amplification, super-resolution and so on. Their precise arrangement, geometrical dimensions and orientation can affect light in a way that is unexpected with conventional materials. The initial research in metamaterials dates back to the late 1960s with the early work of V G Veselago [3], where he theorized a new type of material that can exhibit negative electrical permittivity (ε) and negative magnetic permeability (μ) simultaneously over a common frequency band, thus giving rise to negative refractive index (n).

These materials, commonly called negative index materials (NIMs), remained for long time as 'science fiction' due to the unavailability of such materials in nature. Significant progress has been made through the work of J B Pendry *et al*, who proposed a composite structure exhibiting a negative refractive index. The structure, which combines plasmonic wires (PWs) [4] and split ring resonators (SRRs) [5], paved the way to the first experimental demonstration of the negative refraction in the microwave regime [6]. Later on, a tremendous variety of structures were proposed and contributed favourably to the considerable evolution of this new generation of materials [7 12], and the number continues to grow to this day.

The terahertz (THz) regime, that extends from 100 GHz to 10 THz, is a particularly interesting region, which remained inaccessible for long time due to the absence of appropriate

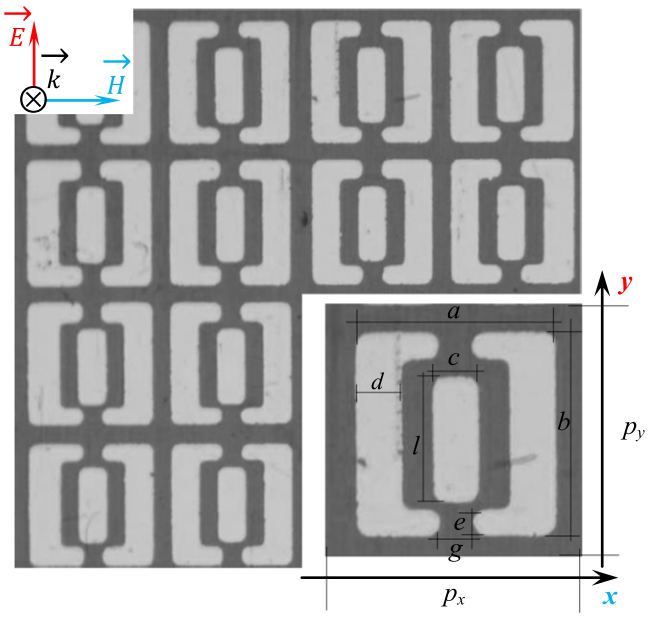

Figure 1. (a) Microscope image of the fabricated metamaterial with the relevant geometrical dimensions $p_x = p_y = 300\ \mu$m, $a = b = 250\ \mu$m, $c = d = 50\ \mu$m, $e = 20\ \mu$m, $g = 50\ \mu$m, $l = 150\ \mu$m, $t_{substrate} = 50\ \mu$m.

emitters and detectors [13]. Recently, this frequency band experienced renewed interest due to advances in semiconductor technology, which gives rise to inexpensive sources and detectors, thus constituting a breakthrough for many useful applications, including subdiffraction imaging [14], cloaking [15], near perfect absorption [16, 17], polarization conversion [18, 19], sensing [20 23] etc.

In this work, we propose a metamaterial based on metamolecules supported by a flexible polymer operating in the terahertz regime. The electromagnetic behavior of the structure has been investigated numerically using the finite element method and experimentally by means of terahertz time domain spectroscopy (THz-TDS). Our results reveal that the metamolecules exhibit an electromagnetic behavior that alternates between rejection and transparency characteristics in the 0.1 1 THz frequency range, potentially suitable for spatial filtering, antennas and sensing applications.

2. Presentation of the investigated metamaterial

The proposed metamaterial is shown in figure 1. The elementary cell of the structure combines an inner cut wire (CW) and an outer two-gap split ring resonator (SRR), made of 200 nm thick aluminum. They are printed on the top side of a 50 μm thick Kapton® substrate using standard optical lithography, with the relevant geometrical dimensions $p_x = p_y = 300\ \mu$m, $a = b = 250\ \mu$m, $c = d = 50\ \mu$m, $e = 20\ \mu$m, $g = 50\ \mu$m, $l = 150\ \mu$m. Considered as the fundamental building blocks of various metamaterials, the SRR and the CW have been widely used for constructing materials with negative permeability, negative permittivity and even negative refractive index when combined together [4 6]. The commercial dielectric substrate Kapton® that was considered in simulations and used in the fabrication process has a relative dielectric permittivity $\varepsilon_r \sim 3$, and a moderate loss level ($\tan\delta \sim 0.05$) up to 2 THz (controlled by THz-TDS). Due to its small thickness, the chosen dielectric spacer has a very good mechanical flexibility, which is highly sought for applications with conformal geometries. The proposed metamaterial is obviously anisotropic and was illuminated by a TM-polarized incidence plane wave (i.e., $E \| CWs$), with a single layer along the direction of propagation k. Note that an infinite structure was considered in the simulations along E and H fields, with a perfect conductor nature of the metallic constituents (SRRs and CWs), while a prototype covering a more realistic surface of about $2 \times 2\ \text{cm}^2$ was fabricated.

3. Numerical simulations and experimental measurements

Numerical simulations based on the finite element method (FEM) were carried out by applying necessary periodic boundary conditions. The elementary cell of the designed metamaterial was placed inside an air box with lateral dimensions of $300\ \mu\text{m} \times 300\ \mu$m and was illuminated by a normally incident plane wave with the electric field parallel to the y-axis and the magnetic field parallel to the x-axis. Perfect electric conductor (PEC) boundary conditions were applied along the y-axis, perfect magnetic conductor (PMC) boundary conditions were applied along the x-axis, and open boundary conditions were applied in the z-direction (direction of propagation k).

Measurements using THz-TDS were made in order to characterize the electromagnetic behavior of the structure. A schematic diagram and a photograph of the THz-TDS setup are shown in figure 2(a). Photoconductive (PC) antennas were used as the emitter and detector of the THz pulses. The excitation source of the PC antennas was a femtosecond fibre laser, whose centre wavelength, repetition rate and pulse width were 780 nm, 80 MHz and 88 fs, respectively. The THz pulses were horizontally polarized and collimated by an off-axis parabolic mirror. The beam diameter was approximately 10 mm on the sample. In the transmission measurements, the incident plane waves are normal to the sample surface and the transmitted THz electric field is calibrated with respect to transmission in free space between the emitter and the receiver.

The simulated (solid line) and measured (hollow circles) frequency-dependent amplitude transmission of the metamaterial slab is shown in figure 2(b), with a very good agreement. One can observe a double transmission window around 0.46 and 0.89 THz. Parametric study performed on the designed metamaterial but not represented here has shown that the response of the metamaterial is determined by the size, the geometry of the elementary cell, the periodicity and the properties of the dielectric substrate.

In order to attempt to understand the origin of the transmission feature, we have further performed numerical simulations separately on the SRR only and CW only (the

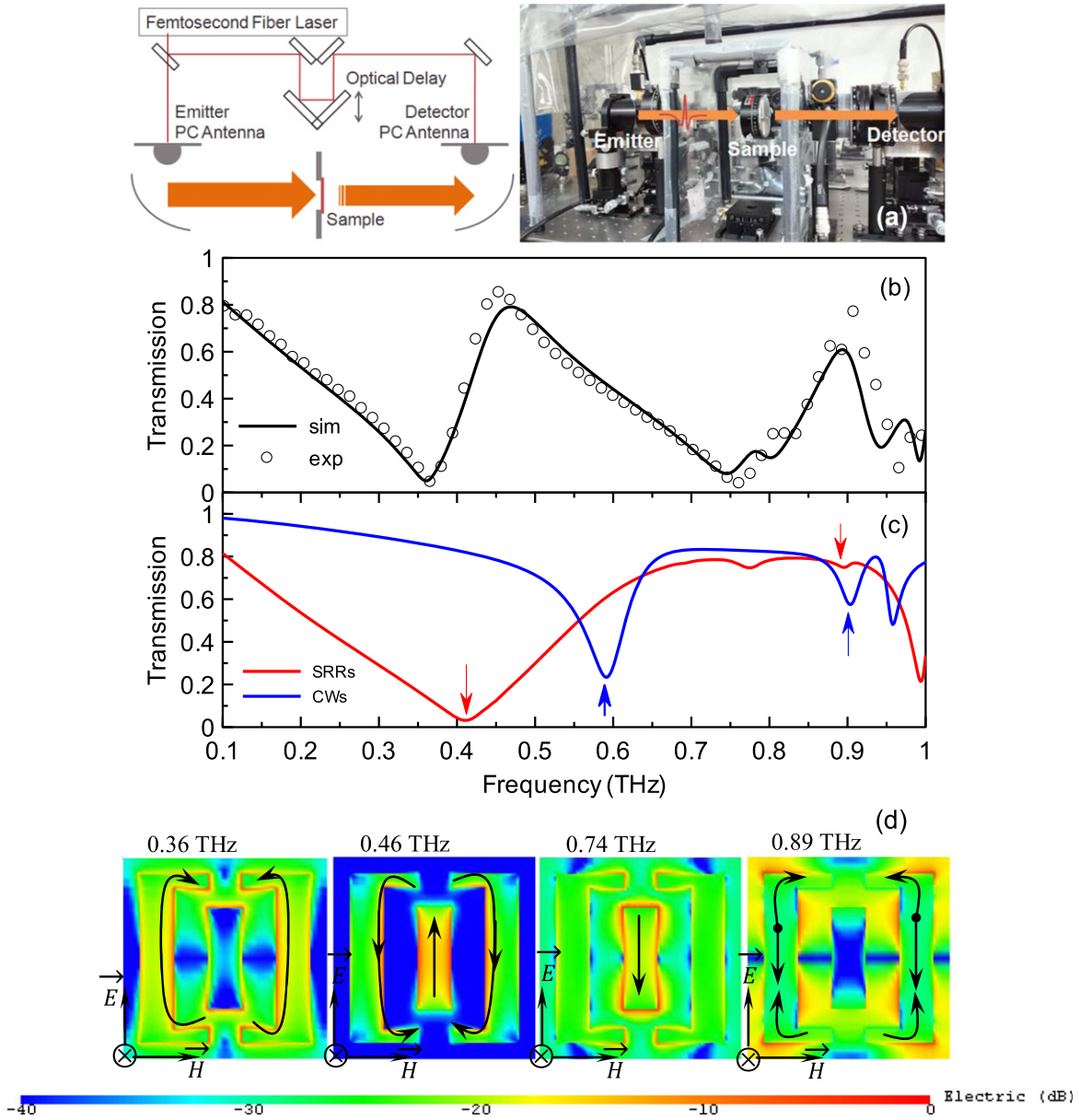

Figure 2. (a) Schematic diagram and photograph of the THz TDS setup used for experimental measurements. (b) Simulated (solid line) and measured (hollow circles) transmission spectrum of the investigated metamaterial. (c) Amplitude of the transmission of SRRs and CWs in the case of TM polarized incidence plane wave ($E \| \text{CWs}$). (d) Electric field amplitudes and surface current directions when driven by the incident field (denoted by black arrows for greater clarity) from left to right at the lower frequency resonance of 0.36 THz, at the transparency peak of 0.46 THz, at the higher frequency resonance of 0.74 THz and at the transparency peak of 0.89 THz.

CW and SRR are removed, respectively). The result of the investigation is shown in figure 2(c). The following statements can be made. (i) Both electromagnetic spectra of SRRs and CWs exhibit a resonant dip at about 0.41 THz for SRRs and around 0.59 THz for CWs (denoted by arrows), with distinct Q factors of about 1.5 and 9.8, respectively (the Q factor is obtained from the transmission curve, $Q = \omega_0/\Delta\omega$, where ω_0 is the resonance frequency and $\Delta\omega$ is the full width at half maximum bandwidth). (ii) Two additional dips appear in the transmission responses of SRRs and CWs (also denoted by arrows). They are weakly pronounced and coincide in frequency around 0.9 THz, thus giving rise to the second transmission window at about the same corresponding frequency of 0.9 THz.

To gain further understanding of the nature of these resonances, we depicted in figure 2(d) the electric field amplitudes and the surface current distributions at frequencies of 0.36, 0.46, 0.74 and 0.89 THz. The directions of the currents on the metallic layer are indicated by black arrows for greater clarity. At the resonant frequency of the transmission dip located at 0.36 THz, the two symmetric current loops at the right and the left arms of the SRR are parallel to each other and highly radiative. The terahertz field scattered from the metamaterial interferes constructively and gives rise to a dipole-like resonance feature. At the frequency of 0.46 THz,

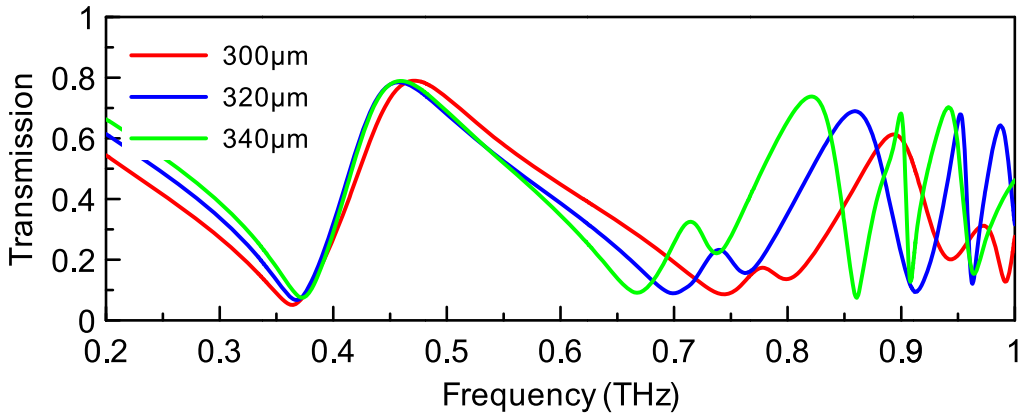

Figure 3. Transmission spectra of the designed metamaterial with different periods $P_x = P_y$.

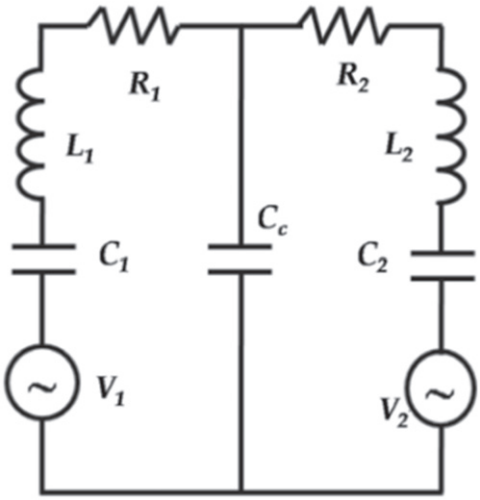

Figure 4. Electric circuit modelling the response of the coupled CW SRR structure.

the structure opens up a transparency window allowing the incident wave to be transmitted with maximum amplitude of about 80%. At the higher frequency resonance of 0.74 THz, we observe the excitation of an electric dipole in the CW and the surface currents of the SRR appear to be suppressed. The currents associated with the transmission peak at 0.89 THz are excited only at the edges of the SRR. One can observe anti-parallel current pairs with nodes at the top and bottom of both vertical arms (right and left) of the SRR.

We have further performed simulations on the designed metamaterial by varying the period $P_x = P_y$ within 300 340 μm while the dimensions of the SRR and CW were fixed. Figure 3 shows the calculated transmission spectra under different periods P. One can observe that the higher-order resonance at 0.74 THz shifts towards lower frequencies as the period P increases, while the changes of the first-order resonance at 0.36 THz is neglected. In short, it is obvious that the first transmission dip at 0.36 THz results from the strong electric resonance in the structure (this is confirmed by the retrieved effective permittivity, but not represented here, which exhibits a highly pronounced Lorentz-like resonance at 0.36 THz), while the second transmission dip at 0.74 THz arises in part from interaction of neighboring unit cells.

A possible modelling of the CW SRR structure as two *RLC* circuits with different lumped elements R_1, L_1, C_1, R_2, L_2 and C_2, coupled by a common capacitor C_c is given in figure 4. The left and the right loops of the circuit represent the CW and the SRR, and contain alternating voltage sources to mimic the excitation of the external electric field.

The *RLC* analysis will be performed by solving equations (1) and (2):

$$\begin{pmatrix} i_1 \\ i_2 \end{pmatrix} = Z^{-1} \begin{pmatrix} v_1 \\ v_1 \end{pmatrix} \tag{1}$$

where v_1 and v_2 are the driving voltages; the impedance matrix Z of the circuit is given by

$$Z = \begin{pmatrix} -\mathrm{i}\omega L_1 + R_1 + \dfrac{1}{-\omega \mathrm{i} C_1} & \dfrac{1}{-\omega \mathrm{i} C_c} \\ \dfrac{1}{-\omega \mathrm{i} C_c} & -\mathrm{i}\omega L_2 + R_2 + \dfrac{1}{-\omega \mathrm{i} C_2} \end{pmatrix}. \tag{2}$$

The lumped elements will be chosen judiciously by fitting the spectra obtained from the numerical simulations [24]. The topology of the proposed structure offers an extra degree of freedom to gain more insight into the coupling mechanisms between the SRR and the CW, by changing the spatial configuration of the metamolecules. Indeed, we have further carried out calculations with various rotating angles θ of the CW. Note that the length l of the CW has been optimized numerically and set to 130 μm in order to achieve the angular study. The resonant dip and peak that initially occur at 0.36 and 0.46 THz are slightly shifted to 0.37 and 0.51 THz, respectively, as illustrated by the dashed black curve of figure 5(a). As we gradually rotate the CW resonator, the modulation of the first transparency peak (0.51 THz) and the second transmission broad dip (0.74 THz) are observed. The first transmission dip at about 0.37 THz is not dramatically affected by the rotation of the CW, except for a minor shift towards high frequencies from 0.37 to 0.41 THz, which corresponds to about 10% of tunability (see figure 5(a)).

The first transmission peak around 0.51 THz changes in intensity and splits into two distinct peaks, which move in

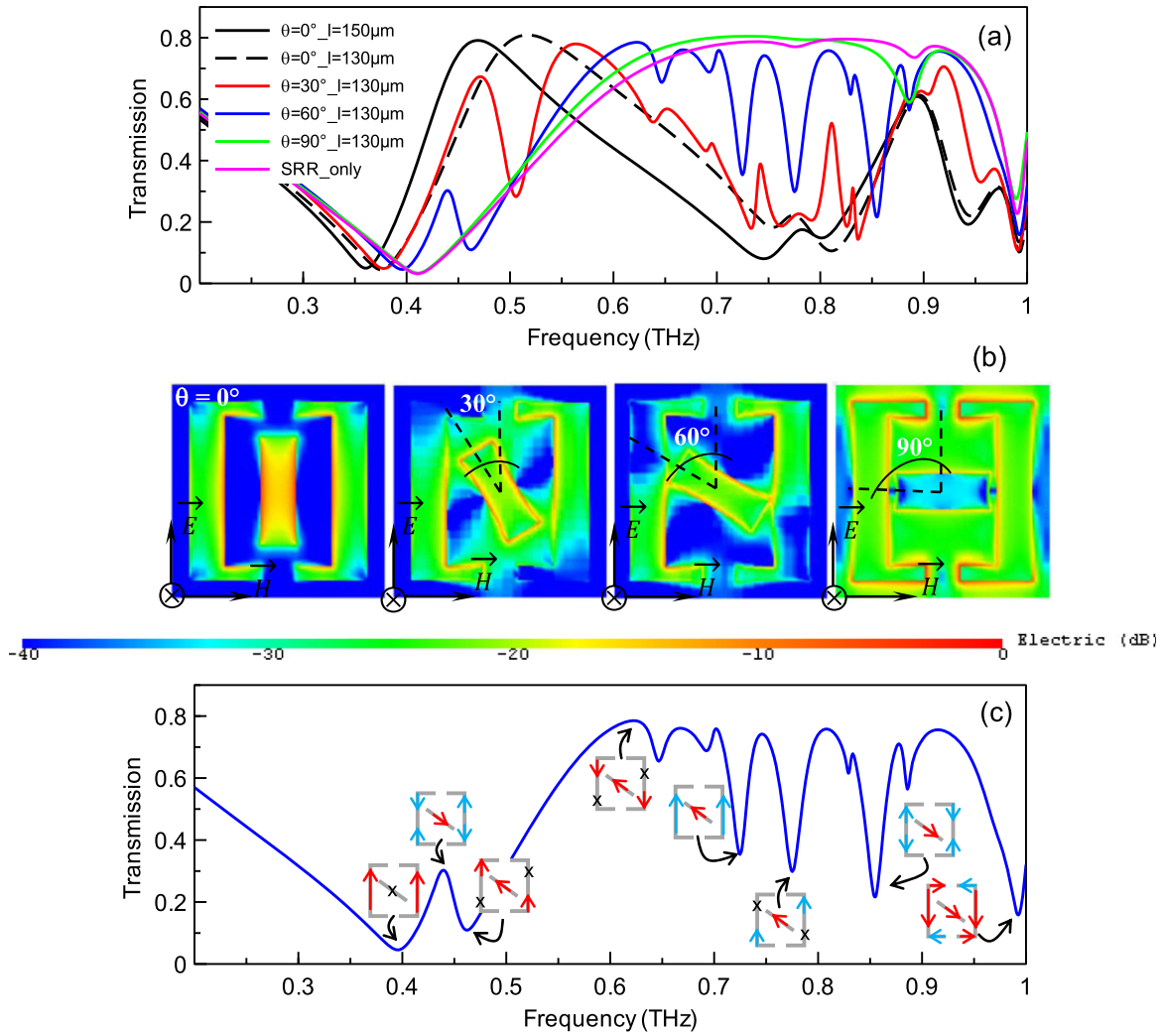

Figure 5. Evolution of the transmission spectra (a) and electric field distribution (b) around the first transmission peak at about 0.51 THz for different rotating angles θ of the cut wires, with $l = 130\,\mu$m. (c) Amplitude of the transmission for the sample with $\theta = 60°$. The symbols represent the distribution of the surface currents in the SRR and the CW at each transmission dip and peak.

opposite directions (see figure 5(a)). In other words, the transparency window around 0.51 THz tends to disappear; this behavior is accompanied by a gradual transfer of energy from the CW to the SRR (see the spatial distribution of the electric field in figure 5(b) for different rotating angles θ, around the transparency peak at about 0.51 THz). For the configuration with $\theta = 90°$, the electromagnetic energy is distributed only on the SRR, which becomes highly radiative. Consequently, the transparency signature disappears and the spectral response of the whole structure is similar to that of the SRR.

The broadband rejection window (i.e., transmission dip at about 0.74 THz) is also affected by the rotation of the CWs. A series of additional transmission peaks and dips appears within this frequency range, thus translating the higher-order multipolar coupling mechanisms that exist between the SRR and CW constituents. In order to illustrate these coupling effects, we have depicted in figure 5(c) the amplitude of the transmission for an intermediate case of $\theta = 60°$. The symbols in figure 5(c) represent the surface currents in the SRR and the CW at each transmission dip and peak.

For a better understanding of the symbols, the red arrows indicate that the surface currents are strongly excited, while the blue arrows indicate a weak excitation of the surface currents. In contrast, a black cross indicates that the constituents or portions of the metamolecules are not solicited by the incident terahertz wave.

4. Conclusion

In conclusion, we have designed, fabricated and experimentally characterized a flexible planar metamaterial operating in the terahertz frequency range. The spectral response of the investigated metamaterial, which exhibits a multiple band frequency response suggests a potential path forward for achieving numerous metamaterials with conformal geometries in the field of antennas, spatial filtering and bio-sensing. Furthermore, the lowering of the symmetry of the unit cell

induced by the angular study appears to be very promising for polarization conversion applications.

Acknowledgments

This work was initiated at the University of Limoges. R Yahiaoui would like to thank MICEL Corporation (www.micel.fr) for providing us with the Kapton® substrate. K Takano, F Miyamaru and M Hangyo were partly supported by a Grant-in-Aid for Scientific Research on Innovative Areas, 'Electromagnetic Metamaterials' (22109003), from the Ministry of Education, Culture, Sports, Science, and Technology (MEXT), Japan.

References

[1] Fang N, Lee H, Sun C and Zhang X 2005 *Science* **308** 534
[2] Schurig D, Mock J J, Justice B J, Cummer S A, Pendry J B, Starr A F and Smith D R 2006 *Science* **314** 977
[3] Veselago V G 1968 *Sov. Phys. Usp.* **10** 509
[4] Pendry J B, Holden A J, Stewart W J and Youngs I 1996 *Phys. Rev. Lett.* **76** 4773
[5] Pendry J B, Holden A J, Robbins D J and Stewart W J 1999 *IEEE Trans. Microw. Theory Tech.* **47** 2075
[6] Shelby R A, Smith D R and Schultz S 2001 *Science* **292** 77
[7] Kafesaki M, Tsiapa I, Katsarakis N, Koschny T, Soukoulis C M and Economou E N 2007 *Phys. Rev.* B **75** 235114
[8] Shalaev V M 2007 *Nature Photon* **1** 41
[9] Valentine J, Zhang S, Zentgraf T, Ulin Avila E, Genov D A, Bartal G and Zhang X 2008 *Nature* **455** 376
[10] Rockstuhl C, Menzel C, Paul T, Pertsch T and Lederer F 2008 *Phys. Rev.* B **78** 155102
[11] Yahiaoui R, Němec H, Kužel P, Kadlec F, Kadlec C and Mounaix P 2009 *Opt. Lett.* **34** 3541
[12] Miyamaru F, Kuboda S, Taima K, Takano K, Hangyo M and Takeda M W 2010 *Appl. Phys. Lett.* **96** 081105
[13] Hangyo M, Tani M and Nagashima T 2005 *Int. J. Infrared Millimeter Waves* **26** 1661
[14] Tuniz A *et al* 2013 *Nat. Commun.* **4** 2706
[15] Gaillot D P, Croënne C and Lippens D 2008 *Opt. Express* **16** 3986
[16] Grant J, Ma Y, Saha S, Khalid A and Cumming D R S *Opt. Lett.* **36** 3476
[17] Yahiaoui R, Guillet J P, de Miollis F and Mounaix P 2013 *Opt. Lett.* **38** 4988
[18] Cong L *et al* 2013 *Appl. Phys. Lett.* **103** 171107
[19] Grady N K *et al* 2013 *Science* **340** 1304
[20] Yoshida H *et al* 2007 *Appl. Phys. Lett.* **91** 253901
[21] Debus C and Bolivar P H 2007 *Appl. Phys. Lett.* **91** 184102
[22] Tao H *et al* 2011 *Adv. Mater.* **23** 3197
[23] Miyamaru F *et al* 2014 *J. Infrared Milli Terahz Waves* **35** 198
[24] Meyrath T P, Zentgraf T and Giessen H 2007 *Phys. Rev.* B **75** 205102